



Optimizing the Flow Electrooxidation of Glycerol Using Statistical Design of Experiments

Rachel N. Gaines,¹ Beth A. Kleimenhagen,¹ James J. Griebler,¹ Lauren C. Harris,² Andrew A. Gewirth,^{2,*} Simon A. Rogers,¹ and Paul J. A. Kenis^{1,3,*}

¹Chemical and Biomolecular Engineering, University of Illinois Urbana-Champaign, Urbana, Illinois, United States of America

²Chemistry, University of Illinois Urbana-Champaign, Urbana, Illinois, United States of America

³International Institute for Carbon-Neutral Energy Research (WPI-I2CNER), Kyushu University, Nishi-ku, Fukuoka, Japan

Many studies have investigated the conversion of biomass derivatives to value-added products. However, the influence of different factors on the reaction outcomes of these often-complex systems is not well understood. Herein, a statistical design of experiments—specifically, response surface methodology—is applied to the glycerol electrooxidation reaction in a flow electrolyzer. Four operational variables (glycerol concentration, NaOH concentration, flow rate, and catalyst loading) were investigated for their effects on measurable responses of the electrochemical reaction: current density and Faradaic efficiency to a given product. Independent optimizations of current density and Faradaic efficiency, as well as simultaneous optimization of both, were investigated. Each optimization was evaluated using response surface coefficients to analyze sensitivity and simulated runs to visualize the parameter space. These evaluations revealed contradictions in operating conditions required to simultaneously maximize current density and Faradaic efficiency to C₃ products glycerate and lactate, leading to low current densities and Faradaic efficiencies. However, simultaneously maximizing current density and Faradaic efficiency to C₁ product formate led to high current densities and Faradaic efficiencies. These insights guide tuning GEOR production to maximize overall reactor performance. Furthermore, this study outlines a framework for experimental evaluation and optimization of other electrolysis chemistries.

© 2024 The Author(s). Published on behalf of The Electrochemical Society by IOP Publishing Limited. This is an open access article distributed under the terms of the Creative Commons Attribution 4.0 License (<http://creativecommons.org/licenses/by/4.0/>), which permits unrestricted reuse of the work in any medium, provided the original work is properly cited. [DOI: 10.1149/1945-7111/ad537c]



Manuscript submitted December 27, 2023; revised manuscript received March 21, 2024. Published June 18, 2024.

Supplementary material for this article is available [online](#)

Valorization of biomass-derived feedstocks is a rapidly growing field that seeks to use renewable feedstocks to reduce greenhouse gas emissions associated with chemical production. Of particular interest is the conversion of biomass derivatives using electrified means, as these conversions can be performed at ambient temperature and pressure, and the scope of possible conversions is broad.^{1,2}

A common biomass derivative is glycerol, a 3-carbon polyol synthesized as a byproduct of biodiesel production. Glycerol can be used as a feed in electrolysis processes for a variety of applications.³ For example, substituting anodic water oxidation with glycerol oxidation, effectively side-stepping the energy-demanding oxygen evolution reaction, can decrease the overall energy consumption of cathodic conversions of interest such as hydrogen production and carbon dioxide reduction.^{2,4–6} Alternatively, glycerol oxidation can be pursued on its own as a way to produce value-added products.^{7,8} Prior work has demonstrated up to twelve possible products from glycerol oxidation, including lactate,^{9–15} glycolate,^{16–18} formate,^{19–25} glycerate,^{26–31} oxalate,^{32–34} and others.^{35–39} Glycerol oxidation-based electrified manufacturing of some of these products may hold promise in terms of economics and life cycle arguments.

Prior work on the glycerol electrooxidation reaction (GEOR) was primarily focused on identifying a single condition, typically a catalyst identity or a catalyst loading that maximizes selectivity to one of those products. Most efforts ascribe product selectivity to the specific catalysts used, across the full spectrum of precious metals,^{10,11,15–18,20,26–28,35,37,38} transition metals,^{9,19,21,22,24,25,32,33} and their combinations with nonmetals.^{12,23,39} Operational conditions for these studies, however, vary widely. pH ranges chosen typically stem from the catalyst used; however, electrooxidation rates are typically higher in base, as deprotonated species are more easily oxidized.^{7,40} Most studies utilize bulk electrolysis cells (e.g., 3-electrode cells, H-cells, W-cells) to maximize selectivity and overall glycerol conversion.^{9–37,39} Far fewer studies utilize flow

electrolyzers, despite flow electrolyzers currently comprising the majority of industrial electrochemical reactors.^{30,38,41} To effectively scale GEOR, especially in tandem with cathodic reactions such as carbon dioxide reduction and hydrogen evolution, a detailed understanding of GEOR in flow electrolyzers must be developed.

Effectively scaling GEOR also requires deeper understanding of the factors influencing reaction *activity* and *stability*, in addition to selecting catalysts for their product *selectivity*. Selectivity, activity, and stability manifest experimentally as, respectively, Faradaic efficiency (FE), current density (CD), and durability, and all three must be equally considered for a reaction to be scalable. Particularly, the activity (CD) of a reaction must be sufficiently high to merit scaling. Exactly what number, and at what scale, equates to “sufficiently high” is still nebulous, with definitions ranging from 100 mA/(mg catalyst) to 1 A/(cm² geometric area).^{8,42,43} However, prior work on electrolysis scalability shows that maximizing CD must be a consideration.^{44–46} Unfortunately, the literature investigating GEOR continues to revolve around maximizing FE through the development of new catalysts, with minimal attention paid to current density. Several of these studies do not report current density at all, or report low numbers in the range of 1–10 mA cm⁻².^{10,12–14,16,18,19,21–23,26–33,35–37} Therefore, investigating how to maximize reaction CD alongside FE (as well as durability; beyond the scope of this study) is critical.

Studies optimizing GEOR outside of catalyst-related experimentation are rare. In bulk electrolysis, the effects of cations and electrolyte composition (i.e., concentration of glycerol and concentration of electrolyte) have been studied.^{15,47,48} In the few flow electrolysis studies, analyses have examined effects of applied current, feed and/or electrolyte flow rate, and electrolyte composition.^{49–51} The variety of catalysts used, combined with the variation in factors investigated, obscures the intertwined effects of these factors on CD and FE. Furthermore, optimizing one-factor-at-a-time conflates local optima with the true global optimum. One way to avoid this is by utilizing a statistical design of experiments to map a larger variable space, while keeping the total number of experiments small.

*Electrochemical Society Fellow.

²E-mail: kenis@illinois.edu

Four prior studies have utilized statistical design of experiments to investigate a range of parameters simultaneously for electrochemical utilization of glycerol.^{52–55} These designed experimentation approaches allow for efficient exploration of the full parameter space to identify global optima. Each of the prior studies uses a variation of Response Surface Methodology (RSM) design of experiments, intended to incorporate curvature into linear regression models based on experimental results of multivariate processes.⁵⁶

Two of these studies were performed in fuel cells.^{52,53} Briefly, these studies investigated the effects of factors including anodic/cathodic electrolyte concentration, temperature, and catalyst loading on current/power density. Interestingly, one study concludes that the most influential factor is temperature, whereas the other asserts that it is electrolyte concentration and catalyst loading.

Two other studies used RSM design of experiments for GEOR in bulk electrolysis: one in an acidic medium, the other in a basic medium.^{54,55} The study exploring GEOR in an acidic medium investigated electrolyte composition and applied current to maximize to either organic acid or “solvent” (i.e., dihydroxyacetone, glycidol) compound classes.⁵⁴ Glycerol concentration ([GLY]) and electrolyte concentration were found to be most influential.

Peralta-Reyes et al. investigated GEOR in a basic medium, using GEOR as a sacrificial anode reaction in parallel with cathodic hydrogen production.⁵⁵ They sought to maximize hydrogen production while minimizing oxygen evolution via factors of temperature, [GLY], and applied current. Applying RSM revealed that [GLY] and the paired interaction between applied current and temperature is most influential to maximize hydrogen production. These same two factors as well as the interaction between [GLY] and temperature are most influential to minimize oxygen evolution. This study, because of its focus on optimizing water electrolysis, did not explore the effects of the various factors on GEOR activity or product speciation.

The GEOR studies that employed RSM designs of experiments demonstrated the utility of RSM to determine optimal operational conditions for different electrocatalytic processes. Those working in fuel cells evaluated the effects of factors on power density or current density, and the electrolysis studies assessed the effects of factors on product speciation, but each study is lacking in an area crucial to the development of GEOR as an electrocatalytic process. Additionally, the choice of and justification for factors and factor ranges across these studies was not consistent. Generally, [GLY] was found to be important, but other factors of interest—and the trends resulting from those factors—varied widely. The same conclusion can be drawn when reviewing related non-RSM research efforts on GEOR.

No investigation to date has *simultaneously* optimized activity and selectivity of GEOR, without influence of one on the other. In other words, no investigation has sought to optimize the current density and Faradaic efficiency of a given product at the same time. Prior work employed either one-factor-at-a-time optimization techniques or RSM techniques for a single outcome. The valorization of biomass-derived feedstocks via electrolytic conversion will require optimization of the electrooxidation process in terms of activity (CD) and selectivity (FE) *simultaneously*. Identifying the most appropriate operating parameters of these electrified processes will be critical to evaluate their potential for reducing emissions of chemical manufacturing.

In this work, we seek to address some of the voids in advancing electrolytic processes for electrified chemical manufacturing. Specifically, we apply Response Surface Methodology (RSM) to the glycerol electrooxidation reaction in flow electrolyzers. The effects of the four primary factors of interest—glycerol concentration, NaOH concentration, electrolyte flow rate, and catalyst loading—are evaluated for their influence on maximizing current density and maximizing of Faradaic efficiency to both glycerate and lactate, two products of interest.

Results & Discussion

Overview.—In this work, we apply Response Surface Methodology (RSM) to the glycerol electrooxidation reaction

(GEOR) on gold (Au) catalysts, in parallel with the hydrogen evolution reaction on the cathode in liquid electrolyte flow electrolyzers. We consider four primary factors (variables) of interest: glycerol concentration ([GLY]), NaOH concentration ([NaOH]), electrolyte flow rate (EFR), and catalyst loading (CL). These factors were selected based on the operation of industrial electrolyzers and preexisting literature for GEOR on Au, which suggested that those four factors would be most influential on the performance metrics of current density and Faradaic efficiency.^{57,58} To determine factor limits, we established feasible flow rate and concentration ranges for our liquid electrolyte flow cell and determined an accessible range of catalyst loadings (see Experimental section). This set our factor ranges as follows: [GLY] and [NaOH], 0.01–4.0 M; EFR, 0.5–2.0 ml min⁻¹; CL, 0.1–1.0 mg cm⁻².

To evaluate Faradaic efficiency of multiple mechanistic pathways, we selected glycerate (GEA) and lactate (LA) as model products of GEOR on Au. GEA is the first base-stable product of GEOR, produced by two electrochemical (E) steps (E-E mechanism). LA is a competing product synthesized after the initial electrochemical (E) step by a chemical (C) decomposition step (E-C mechanism).⁵⁹ While GEA and LA have been studied as co-products and individual products of GEOR, tuning the reaction to produce one or the other selectively remains a challenge.^{11,42,60}

We chose three distinct responses for which we evaluated our model: total current density (CD), Faradaic efficiency (FE) for GEA, and FE for LA. The work is thus reported in three sections: (1) Optimizing total CD, irrespective of product speciation; (2) Optimizing FE to GEA or FE to LA separately; (3) Optimizing CD simultaneously with the FE for either GEA or LA. While the experimental approach described here pertains to GEOR specifically, we posit that the employed RSM approach can be employed broadly to other systems, including any electrolysis chemistry.

Application of response surface methodology to GEOR.—Response surface methodology (RSM), particularly a Central Composite Inscribed design, was chosen as the appropriate design of experiments for this study, following the NIST Engineering Statistics handbook.⁵⁶ This design was chosen as it (1) covers the experimental factor space of interest without creating impossible conditions (e.g., negative flow rates); (2) identifies curvature present in the factor space; (3) creates an inherently interpretable (so-called “clear-box”) model; (4) identifies optimal operating conditions. In this section, we describe the model employed in broad strokes, while a detailed description and interpretation of each part of the model can be found in the Experimental section.

For an RSM involving four factors—here represented by the lowercase letters a, b, c, and d—the model takes the form of Eq. 1.

$$\begin{aligned} \text{Response} = & Aa + Bb + Cc + Dd + Eab + Fac + Gad + Hbc \\ & + Ibd + Jcd + Ka^2 + Lb^2 + Mc^2 + Nd^2 \end{aligned} \quad [1]$$

To evaluate the results of the model, we highlight four key features. The first two (quadratic terms, response surface coefficients) come from the form of Eq. 1; the second two (simulated runs, optimal operating conditions) come from the software itself. Each feature is described briefly below.

First, the model includes quadratic terms that illustrate the curvature/nonlinearity of each factor, both in each variable’s interaction with each other variable, as well as the paired interaction with itself. Including these quadratic terms is critical because we expect some kind of optimum point (i.e., a peak) in each of these factors, which would introduce curvature.

Second, each term in the model is weighted by a coefficient (indicated by the capital letters A–N in Eq. 1), which are the model’s Response Surface Coefficients (RSCs). They demonstrate the relative influence of each factor in the model, akin to a sensitivity analysis. The magnitude of each RSC represents its influence on the

Table I. Results and operating conditions for each quantitative optimization, including those predicted by the model and those experimentally obtained. Note that the parentheticals under “Maximize FE to GEA” indicate predictions/results at 0.01 M NaOH.

	Parameter	Optimization				
		Maximize CD	Maximize FE to GEA	Maximize FE to GEA with 4 M NaOH	Maximize FE to LA	Maximize CD & FE to GEA
<i>Results: Predicted by Model</i>	CD (mA/cm ²)	-181.2	N/A	N/A	N/A	-97.1
	FE to GEA (%)	N/A	43.3 (44.4)	19.4	16.9	23.5
	FE to LA (%)	N/A	11.9 (N/A)	29.2	30.7	N/A
<i>Results: Experimentally Obtained</i>	CD (mA/cm ²)	-162.0	-10.4 (-1.4)	-63.2	-51.5	-68.5
	FE to GEA (%)	N/A	36.6 (20.5)	13.3	13.7	23.4
	FE to LA (%)	N/A	0.7 (N/A)	17.5	20.5	N/A
<i>Operating Conditions: Predicted by Model</i>	Cell Potential (V)	-1.4	-0.4	-0.4	-0.4	-1.2
	[NaOH] (M)	3.3	0.1 (0.01)	4.0	4.0	2.4
	[GLY] (M)	1.8	2.2	2.2	2.0	2.3
	EFR (mL/min)	1.4	1.4	1.4	1.1	1.8
	CL (mg/cm ²)	0.8	0.5	0.5	0.6	0.3
	[NaOH] (M)	3.3	0.1 (0.01)	4.0	4.0	2.3
<i>Operating Conditions: Experimentally Obtained</i>	[GLY] (M)	1.8	2.2	2.2	2.0	2.4
	EFR (mL/min)	1.4	1.4	1.4	1.1	1.8
	CL (mg/cm ²)	0.8	0.5	0.5	0.5	0.3

response. The sign of the RSC indicates the direction of change of the response. For a more detailed explanation, the reader is referred to the Supplementary Information (Section SI).

Third, the modeling software can generate any number of *simulated* “experiments” (herein termed “simulated runs”), giving insight to the patterns in the full experimental parameter space. These insights can be easily compared to prior work. The parameter space can also be evaluated for alternative factor settings that can be used to generate similar responses.

Finally, the software identifies factor combinations that give an optimal response (i.e., maximum current density, maximum Faradaic efficiency, or both) for each applied cell potential. This is typically highlighted as the only outcome when using RSM. That said, it becomes much more powerful when evaluated in the context of the other three features described above, the RSCs, the simulated runs, and the model curvature.

To employ the RSM approach, a certain number of actual experiments (based on the factor ranges) must be performed, generating a training set from which the model derives its insights. For this study, each training set comprised 30 experiments with differing conditions. This training set was used at 7 different cell potentials (-0.2, -0.4, -0.6, -0.8, -1.0, -1.2, -1.4 V), each of which was assigned its own sub-model and evaluated independently. Thus, a total of 210 unique experimental conditions was tested. Distributed within this training set were six replicate centerpoint runs (i.e., experimental conditions in the middle of each factor range), the variability of which yielded total model variability, as expressed in the error bars in the model predictions. Factor settings and the results of each of the sets of 30 experiments (CD, half-cell potential, FE to a variety of products) can be found in the supplementary information (Tables S1–S3). In summary, each model for the three optimizations described below was obtained using the full dataset resulting from the seven cell potentials tested for each of the 30 experimental conditions.

The reader may wonder why the objective of this work could not be achieved with a p-value analysis. Indeed, we do *not* use p-values as a metric in our evaluation of the models, in contrast to previous studies. Because our sample size is small (30 experiments) and our HPLC spectra require deconvolution, analyzing solely by p-value would significantly bias our analysis.⁶¹ In this work, we chose to

evaluate the relative influence of each factor on the response and apply (electro-) chemical intuition to evaluate those results. A more detailed discussion can be found in the Supplementary Information (Section SII).

In lieu of p-values, we evaluate the model’s results using the hallmarks of the RSM approach: RSCs, simulated runs, and experimental testing of optimum factor combinations. We test these for three separate types of optimizations in the next three sections: (1) current density only, (2) Faradaic efficiency only, and (3) both current density and Faradaic efficiency simultaneously.

Apply RSM to optimize current density only.—In our first optimization, we identified optimal conditions for maximization of total current density alone in our liquid-electrolyte flow cell. The RSM model obtained for optimization of current density (Table S5) predicted a maximum CD of 181 mA cm⁻² at factor settings of [GLY] = 1.80 M, [NaOH] = 3.30 M, catalyst loading (CL) = 0.83 mg cm⁻², and flow rate (EFR) = 1.41 ml min⁻¹ at -1.4 V cell potential (Table I). We then tested this outcome by running the cell at these factor settings, which yielded a CD of 162 mA cm⁻², in good agreement with the standard deviation based on the variation in the six centerpoint experiments (Fig. 1).

Analysis of the RSCs produced by the model for the optimization of current density alone reveals three terms with outsized effects: [NaOH], [NaOH]², and [GLY]² (Fig. 2). The RSC for [NaOH] is positive, indicating that as [NaOH] increases, current density increases; meanwhile, the RSC for [NaOH]² is negative, indicating the existence of an optimum point between the minimum and maximum of the range. The combined effects of [NaOH] and [NaOH]² on current density likely mimic logarithmic growth, with CD leveling off beyond [NaOH] = 3 M. For comparison, a p-value-based analysis (Table S4) would reveal only a significant influence of [NaOH] and not of [NaOH]² and would therefore not capture the effect plateauing. The RSC for [GLY]² is large, relative to the RSC for [GLY] (Fig. 2). This suggests that the effect of [GLY] on CD resembles a “pure” inverse quadratic relationship, with an optimum in between the minimum and maximum factor settings.

Figure 3 provides a graphical representation of the CDs predicted for 1000 simulated runs as a function of [NaOH] and [GLY] parameter space, for a cell potential of -1.4 V. Because of the

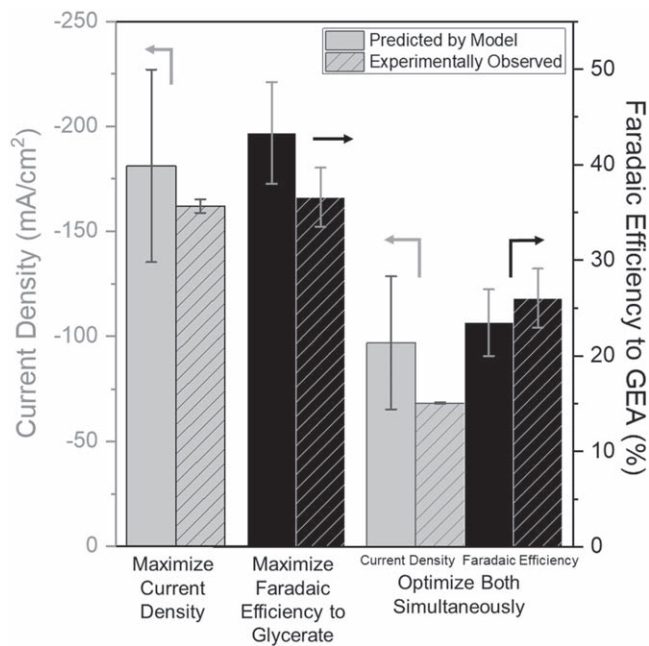


Figure 1. Comparison between the optimal results predicted by the RSM model and the experimental results obtained during experimental testing of the predictions. Three separate optimizations were performed: maximization of current density only, maximization of Faradaic efficiency to glycerate only, and maximization of both current density and Faradaic efficiency to glycerate simultaneously.

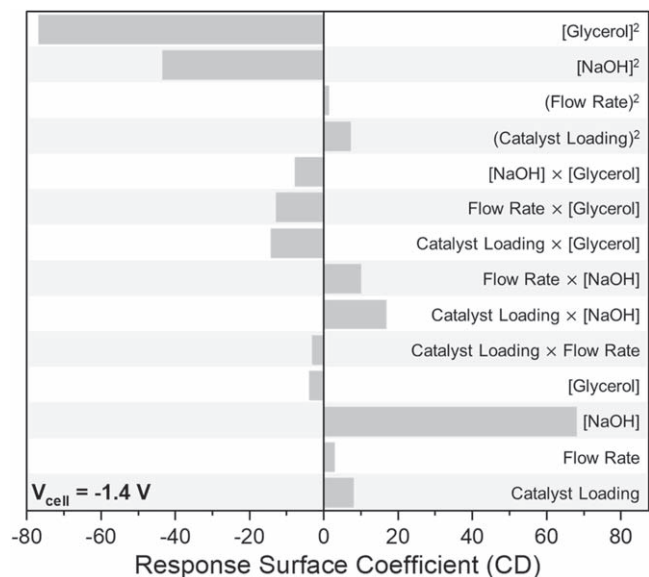


Figure 2. Response surface coefficients generated by the RSM model for the maximization of current density only. The model is most sensitive to $[\text{glycerol}]^2$, $[\text{NaOH}]^2$, and $[\text{NaOH}]$.

dependencies described above, one can see that the CDs of the simulated runs increase with $[\text{NaOH}]$ until about 3 M, but then plateau, and that the CDs exhibit an optimum for intermediate $[\text{GLY}]$. Indeed, a zone of highest current density—over 150 mA cm^{-2} —is predicted to occur with high $[\text{NaOH}]$ (above 3 M) and intermediate $[\text{GLY}]$, between 1 and 3 M.

Prior work has shown that increased $[\text{NaOH}]$ leads to increased current for GEOR on Au catalysts.⁴⁸ High $[\text{NaOH}]$ (i.e., high pH) is important to GEOR on Au for two reasons: (i) it hydroxylates and thus activates the gold catalyst to $\text{Au}(\text{OH})_{\text{ads}}$, the putative active site

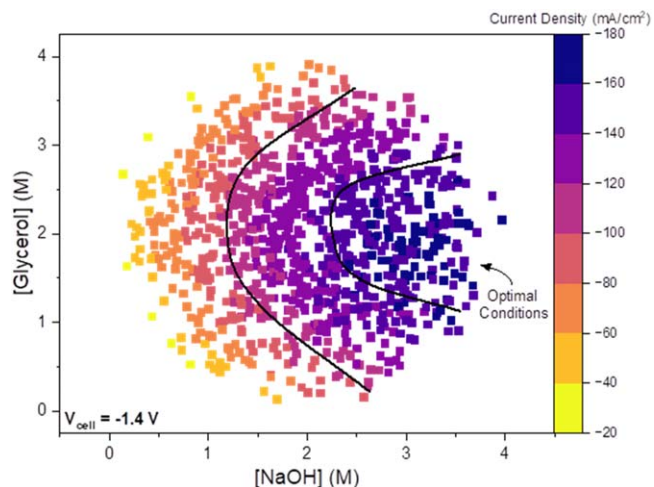


Figure 3. Interaction plot of the two most influential factors on current density: $[\text{NaOH}]$ and $[\text{glycerol}]$. Optimal conditions for maximizing current density are seen at $[\text{NaOH}]$ above 2.5 M when $[\text{glycerol}]$ is between 1 and 3 M.

for GEOR; (ii) it facilitates the deprotonation of glycerol to a glyceroxy anion, $\text{C}_3\text{H}_7\text{O}_3^-$, the primary reactant on Au surfaces.^{20,62,63}

The reason for intermediate $[\text{GLY}]$ to yield high CD can be traced back to Au passivation mechanisms. Under high $[\text{NaOH}]$ and at high potentials, like the -1.4 V used here, $\text{Au}(\text{OH})_{\text{ads}}$ can easily be passivated through oxidation to $\text{Au}(\text{OH})_3$, Au_2O_3 , and AuOOH , none of which are active for GEOR.^{62,63} However, prior work has been shown that increased $[\text{GLY}]$ can delay the onset of Au surface oxidation.⁶² None of the evaluated catalysts herein show any surface-bound oxygen atoms (Table S5, Figs. S4–S5), and are saturated with Au atoms, indicating that the optimum operating conditions avoid surface passivation. In contrast, at high $[\text{GLY}]$, the fraction of deprotonated GLY is lower, reducing reaction rate, which corresponds to lower predicted and observed CDs.

Apply RSM to optimize faradaic efficiency to either GEA or LA.—In our second optimization, we identified optimal conditions for maximization of Faradaic efficiency to glycerate (GEA). The RSM model obtained for optimization of the FE to GEA predicted 44% FE to GEA at factor settings of $[\text{GLY}] = 2.24 \text{ M}$, $[\text{NaOH}] = 0.01 \text{ M}$, $\text{CL} = 0.52 \text{ mg cm}^{-2}$, and $\text{EFR} = 1.36 \text{ mL min}^{-1}$ at -0.4 V cell potential (Table I). We then tested this outcome by running the cell at these factor settings, yielding a FE for GEA of only 23%. This discrepancy can be explained as follows: at this extremely low $[\text{NaOH}]$ of 0.01 M, GEOR on Au catalysts cannot proceed effectively due to insufficient glycerol deprotonation and hydroxylation of the Au surface.^{20,59} To alleviate this effect, we tested the same set of optimal conditions predicted by the model, but with a $[\text{NaOH}]$ of 0.1 M (Table I), yielding a FE for GEA of 36% (Fig. 1). The predicted FE for GEA at this $[\text{NaOH}]$ of 0.1 M is 43%, well within the standard deviation based on the variation in the six centerpoint experiments. Note that $[\text{NaOH}] = 0.1 \text{ M}$ provides acceptable GEOR levels as evident from the tenfold increase in current density (Table I).

RSCs indicate that $[\text{NaOH}]$ has a large negative influence on FE to GEA. To a lesser extent, the RSCs for $[\text{NaOH}]^2$, $\text{EFR} \times [\text{GLY}]$, $[\text{GLY}]$, and EFR all also influence FE (Fig. 4). The negative sign of the RSC for $[\text{NaOH}]$ demonstrates that, primarily, FE to GEA decreases with increasing $[\text{NaOH}]$; in combination with the weaker positive sign of $[\text{NaOH}]^2$, the net result resembles an exponential decay. The influence of both $[\text{GLY}]$ and EFR alone are positive, indicating that increasing (decreasing) either one of them independently *should* result in an increase (decrease) in FE to GEA. However, the negative sign of the interaction term $\text{EFR} \times [\text{GLY}]$

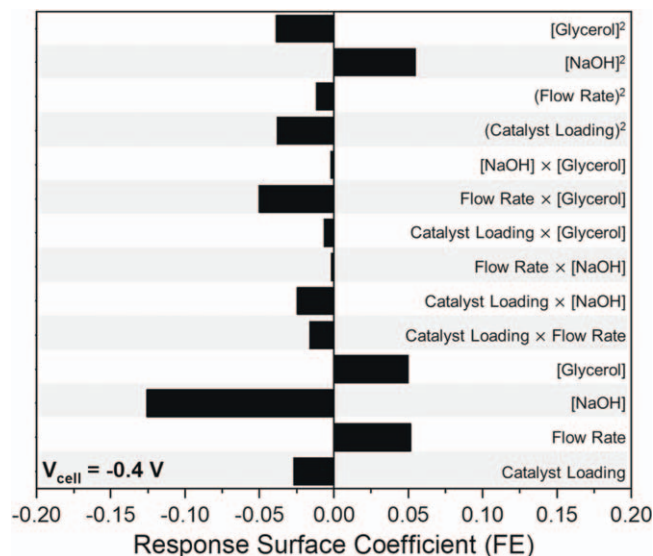


Figure 4. Response surface coefficients generated by the RSM model for the maximization of Faradaic efficiency to glycerate only. The model is most sensitive to $[\text{NaOH}]^2$, flow rate \times [glycerol], [glycerol], [NaOH], and flow rate.

indicates that increasing (or decreasing) *both* [GLY] and EFR *simultaneously* will reduce each variable's ability to increase FE to GEA. Hence, each variable can be neither too high nor too low to maximize FE to GEA.

Figure 5a provides a graphical representation of the FEs for GEA predicted for 1000 simulated runs as a function of the parameter space of [NaOH], [GLY], and EFR, for a cell potential of -0.4 V. This 3D plot reveals the dominating influence of [NaOH] and [GLY]: FE increases significantly with decreasing [NaOH] and at intermediate [GLY]. The influence of EFR is less pronounced: high and low EFRs are encountered throughout the [NaOH] and [GLY] parameter space. Interestingly, the zone with highest FE to GEA—low [NaOH] and intermediate [GLY] range—the EFRs are in the intermediate range. These observed trends are echoed in the interpretation of the RSCs above (Fig. 4).

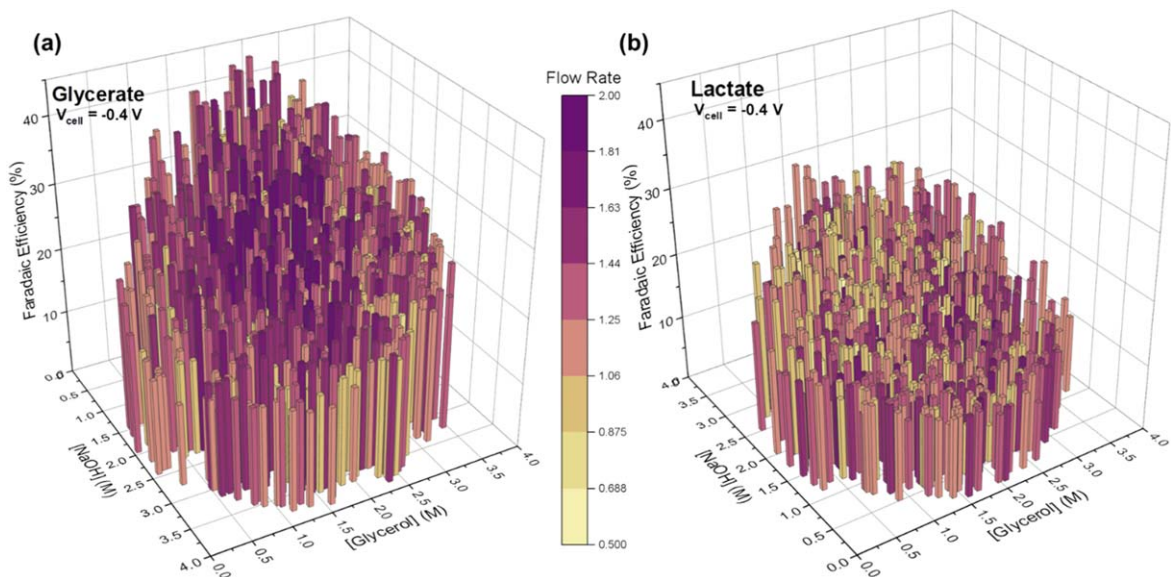


Figure 5. Interaction plot of the three most influential factors on Faradaic efficiency: [NaOH], [glycerol], and flow rate. Note that the axes of [NaOH] are reversed in (a) vs (b) for data visibility. (a) Optimal conditions for maximizing Faradaic efficiency to glycerate are seen at [NaOH] less than 0.5 M when flow rates are above 1.25 ml min⁻¹ and [glycerol] is between 1 and 3 M. (b) Optimal conditions for maximizing Faradaic efficiency to lactate are seen at [NaOH] above 3.5 M when flow rates are below 1.25 ml min⁻¹ and [glycerol] is between 1 and 3 M.

The trends observed in this model for optimization of FE to GEA agree with the mechanistic underpinnings of GEOR. Prior work has shown that chemical (C) and electrochemical (E) steps compete in GEOR on Au.^{11,20,59} The pathway to synthesize glycerate involves two electrochemical steps (“E-E”). However, this E-E pathway competes with an E-C pathway that synthesizes lactate. In particular, the production of lactate is reported to occur at increased rates under high concentrations of base, attributed to the fact that the chemical mechanism is a base-catalyzed Cannizzaro reaction.¹¹ This same trend also is evident in the optimization of FE for Lactate (*vide infra*).

Next, we attempted to follow the same approach to identify optimal conditions for maximization of Faradaic efficiency to lactate (LA). The data obtained from the sets of training experiments exhibited high variability due to an experimental issue. Determining the FE for any of the products formed requires analysis of the HPLC chromatograms. The peak for lactate is convoluted with the peaks for 3 other compounds: DHA, glycolate, and unreacted glycerol. Automated deconvolution methods still led to run-to-run variability between 10 and 40% (Table S3.2). The RSM approach fails to produce statistically relevant predictions for FEs to LA ($p > 0.05$; Table S7) due to these large errors in the experimentally determined FEs to LA at different centerpoints. Thus, we do not compare the model's predicted optimal performance and the corresponding validation experiment, as visualized for other optimizations in Fig. 1. For the same reason, we do not provide an analysis of RSCs for FE to LA, as provided for FE to GEA in Fig. 4. We still provide Fig. 5b, a graphical representation of the FEs for LA predicted for 1000 simulated runs as a function of the parameter space of [NaOH], [GLY], and EFR, for a cell potential of -0.4 V. While these predictions cannot be used with confidence for quantitative predictions (*i.e.*, determining a set of operation parameters yielding optimal FE to LA), the information can be used qualitatively to predict *parameter space ranges* of high performance.

The trends observed in this model for optimization of FE to LA can also be interpreted based on mechanistic underpinnings. The highest FEs to LA occur at the highest [NaOH] (Fig. 5b). Note that the EFRs leading to best performance in FE are generally lower for optimization to LA than to GEA, as evident from the predominantly much lighter bars in Fig. 5b vs Fig. 5a. The lower EFRs (*i.e.*, longer reactor residence times) for optimization to LA indicate that the

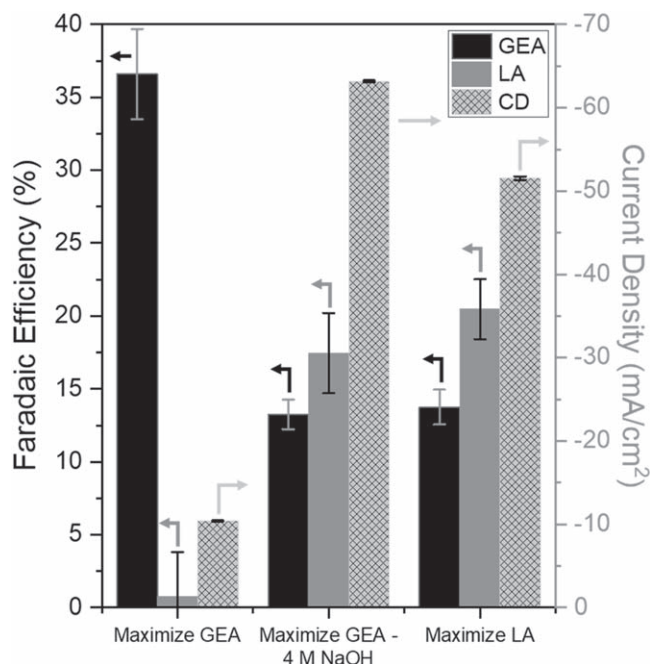


Figure 6. Demonstration of the effect that tuning [NaOH] has on product speciation in glycerol electrooxidation at -0.4 V. Optimization for maximizing glycerate results in 36% Faradaic efficiencies to glycerate and under 1% Faradaic efficiency to lactate with 10 mA cm^{-2} current density. Conversely, optimization for maximizing lactate results in 14% Faradaic efficiency to glycerate and 20% Faradaic efficiency to lactate with over 50 mA cm^{-2} current density. Testing the same set of optimization conditions for maximizing glycerate but changing the [NaOH] from 0.1 M to 4 M results in Faradaic efficiencies and current densities akin to that of the optimization for maximizing lactate.

chemical step of the E-C mechanism requires additional time to proceed. Conversely, the higher EFRs, i.e. shorter reactor residence times, for optimization to GEA indicate the second electrochemical step of the E-E mechanism requires less time to proceed. These trends are in good agreement with both prior work^{11,20,59} and with the quantitative model for FE to GEA (*vide supra*).

Next, we compared the results for optimization of the FEs to GEA and to LA. The operational parameter range of optimum performance for both is different, with the major difference being the [NaOH] range. Thus, we decided to test the effects of [NaOH] on product speciation to ascertain whether [NaOH] was the driving factor in speciation between the E-E and E-C pathways of GEOR. Using the model of FE to LA, despite its aforementioned lack of accuracy, to identify an approximate range of optimal operating conditions for production of LA, we found factor settings of [GLY] = 2.0 ± 0.5 M, [NaOH] = 4.0 ± 0.3 M, catalyst loading (CL) = $0.6 \pm 0.1 \text{ mg cm}^{-2}$, and flow rate (EFR) = $1.1 \pm 0.2 \text{ ml min}^{-1}$ at -0.4 V cell potential (Table 1). The ranges were determined by looking at the 1000 simulated runs and determining the optimum range as the FE maximum $\pm 5\%$. Running the cell at these factor settings yielded a FE to LA of 20%, a 20-fold increase from the FE to LA of under 1% found optimizing for FE to GEA (Fig. 6). At these conditions, the FE to GEA decreased by 22% (from 36% to 14%). Running the cell at optimal factor settings predicted for optimization of the FE to GEA, yet with a [NaOH] of 4 M (optimum for LA) instead of 0.1 M, yielded a FE to LA of 17% and an FE to GEA of 13% (Fig. 6). These FE values for GEA and for LA are nearly identical to those obtained using optimal operating conditions for FE to LA, indicating that the differences in other factors are of minimal influence when tuning the pathway of GEOR on Au. This further underscores that low [NaOH] promotes the E-E pathway that produces GEA, and high [NaOH] promotes the E-C pathway that produces LA.

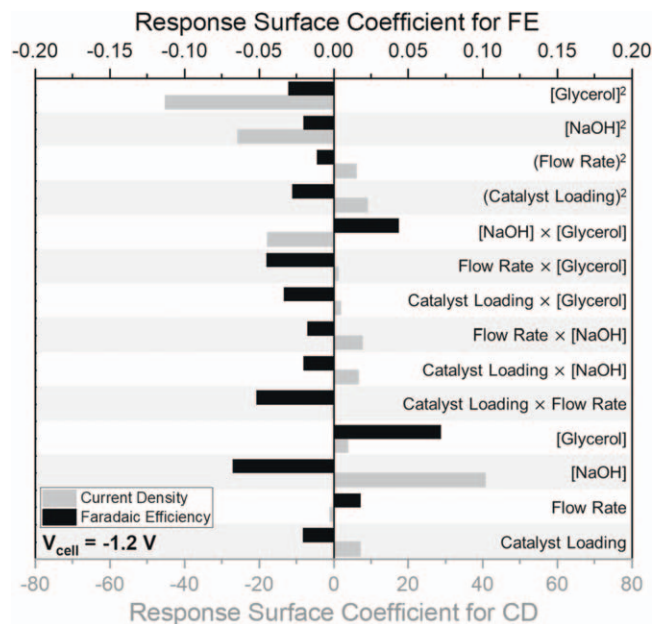


Figure 7. Response surface coefficients generated by the RSM model for the simultaneous maximization of both current density and Faradaic efficiency to glycerate. The model is most sensitive to [glycerol]², [NaOH]², [NaOH] × [glycerol], catalyst loading × flow rate, [glycerol], and [NaOH].

Apply RSM to optimize current density and faradaic efficiency simultaneously.—In our final optimization, we sought to identify optimal conditions for simultaneous maximization of current density and Faradaic efficiency to GEA, and compare these results to simultaneous optimization to LA. The RSM model obtained for simultaneous optimization of CD and FE to GEA (Table S10) predicted a maximum CD of 97 mA cm^{-2} and maximum FE to GEA of 23% at factor settings of [GLY] = 2.27 M, [NaOH] = 2.40 M, CL = 0.27 mg cm^{-2} , and EFR = 1.81 ml min^{-1} (Table 1). Running the cell at these factor settings yielded an experimentally observed CD of 69 mA cm^{-2} and an FE to GEA of 23%, in good agreement with the standard deviation based on the variation in the six centerpoint experiments (Fig. 1). Crucially, these conditions to optimize CD and FE simultaneously occur at a different cell potential (-1.2 V) than the optimizations for current density alone (-1.4 V) or Faradaic efficiency to GEA alone (-0.4 V), indicating optimization for one response or the other, unsurprisingly, does not necessarily lead to optimal conditions for both responses.

RSCs for simultaneous optimization of CD and FE to GEA indicate that all four factors meaningfully influenced the responses (Fig. 7). While [GLY], [GLY]², [NaOH], and [NaOH]² have the largest influences, CL × EFR, EFR × [GLY], and [NaOH] × [GLY] are also relevant. The opposing influence of some of the factors is notable: [NaOH] × [GLY] is positive for FE, but negative for CD; [NaOH] is positive for CD, but negative for FE; and CL × EFR is negative for FE, but essentially zero for CD. Figure 7 also demonstrates the difficulty of pinpointing optimal operating conditions for GEOR: when every factor matters, testing all of them one-factor-at-a-time becomes impractical. A statistical method such as RSM helps in understanding the interdependencies of the reaction, and in selecting operating conditions that lead to the most desirable, feasible performance.

To quantitatively interpret the results of the multi-objective optimization for CD and FE to GEA, we plot the simulated responses of CD and FE to GEA against each other (Fig. 8a). For each simulated data point for a specific FE and CD combination, the model calculates a “desirability” value based on user-inputted maximum and minimum values. Hence, the absolute value of “desirability” is arbitrary, but relative values are of interest.

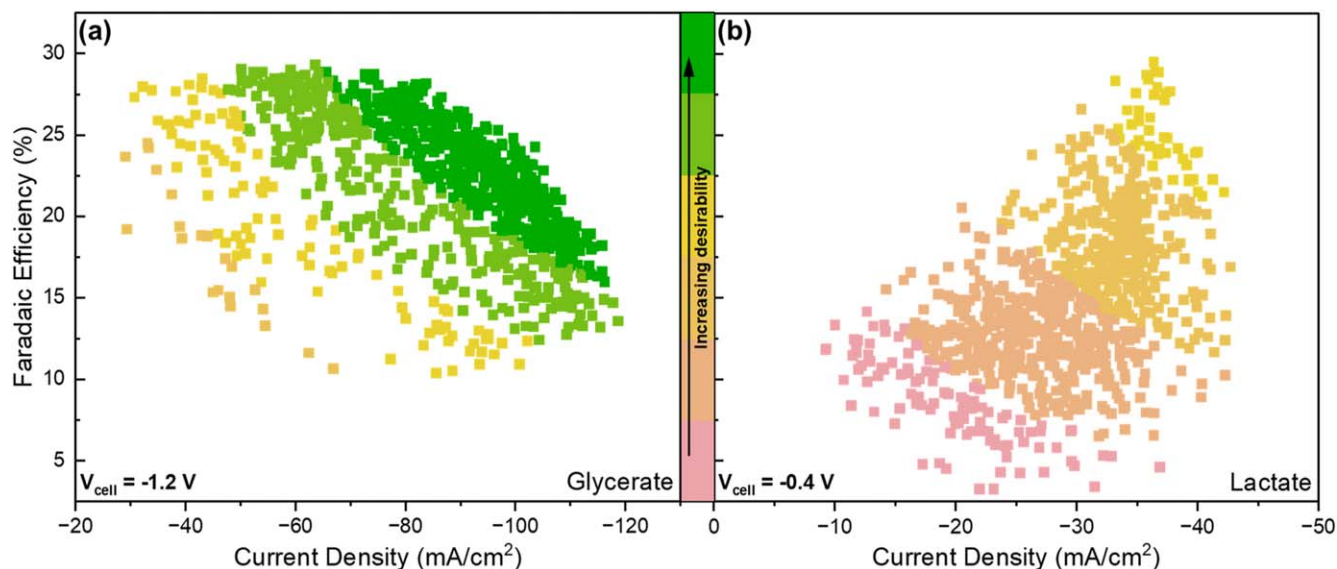


Figure 8. Pareto fronts for simultaneous optimization of current density and Faradaic efficiency to (a) glycerate and (b) lactate. Simultaneous optimization of current density and Faradaic efficiency to glycerate is more desirable due to higher achievable current densities. Conversely, simultaneous optimization of current density and Faradaic efficiency to lactate is less desirable due to lower achievable current densities.

Figure 8 uses the same values for both plots; input values can be found in the supplementary information (Tables S5–S10). Figure 8a reveals that for GEA the responses align themselves in a curve, with the most “desirable” points on the top-right of the plot. This curve, a Pareto front, represents the limits of the optimization. The graph indicates an “optimum front” roughly connecting CD and FEs of 75 mA cm^{-2} and 26% to 115 mA cm^{-2} and 15%. Increasing one value within this range leads to a gradual decrease of the other value (trade off). The optimum of 97 mA cm^{-2} CD and 23% FE to GEA predicted by the model is indeed on this front and was confirmed experimentally (*vide supra*; Fig. 1). As discussed above, the performance limit results from the two responses’ opposite requirements for [NaOH]. With current density requiring high [NaOH] and FE to GEA requiring low NaOH, any optimization for high activity will require significant reductions in overall selectivity to GEA. Conversely, optimization for selectivity to GEA will reduce activity.

We then sought to identify optimal conditions for simultaneous maximization of current density and Faradaic efficiency to LA. From above, we know that optimizing CD as well as optimizing FE to LA requires high [NaOH]. The model for simultaneous optimization of CD and FE to LA (Fig. 8b) showed that the optimal conditions for maximizing CD and FE to LA are observed for a much lower cell potential (-0.4 V) than the optimum for CD and FE to GEA (-1.2 V , Table S10). The plot of the 1000 simulated responses of CD and FE to LA (Fig. 8b) looks very different from the equivalent plot for GEA (Fig. 8a). Whereas the latter exhibits Pareto optimality along a range of CD and FE to GEA combinations, the former exhibits a very narrow range of optimum CD and FE to LA combinations, more akin a Pareto “point” at a CD of approximately 35 mA cm^{-2} and a FE to LA of 30%. In either direction away from the optimum Pareto “point,” the value of the other response drops off. Furthermore, for LA, the achievable current densities are significantly lower due to operation at much lower potentials. Increasing to higher potentials does not lead to improvements in current density and FE to LA simultaneously (Tables S9 and S10).

At -0.4 V , the optimization for FE to LA, as well as the experiment using the factor settings for optimum FE to GEA with high [NaOH], both demonstrate markedly higher CD than the optimization for FE to GEA (51 and 63 vs 10 mA cm^{-2} , respectively; Fig. 6). Despite this improvement in CD, the FEs for LA remain significantly lower than the FEs to GEA at the same potential. Any higher potential decreases the predicted FE to LA by up to half, with minimal increase—if at all—to CD (Table S10).

These seemingly contradictory results demonstrate that FE to LA and CD cannot be improved with increasing potential. Alongside the odd shape of the response for simultaneous optimization of CD and FE to LA (Fig. 8b), these conflicts can be understood when looking at the mechanism of GEOR to LA on Au. Production of LA relies on the unstable product of an electrochemical step that is common to both GEA and LA production. This intermediate must chemically decompose to form LA. LA production is optimized using low EFR (high residence time), but a long residence time also provides the opportunity for both the unstable intermediate and any formed LA to electro-oxidize further to GEA and to acetate/formate, respectively, as visualized in Fig. S1. To minimize the latter pathways, the system must be operated at low potential; minimizing these pathways also reduces electro-oxidative activity, suppressing CD. This effort to simultaneously optimize CD and FE to LA demonstrates the difficulty in producing LA selectively and with high activity.

While applying the RSM approach to simultaneously optimize the CD and FE (to LA or GEA) yielded an understanding of the possible maximum achievable selectivity and rate combinations, it also highlighted that achieving high overall selectivities (i.e. over 50%) seems to be impossible when performing GEOR under the conditions tested (Au catalysts, flow electrolysis cell, operational ranges as specified above). We focused on glycerol oxidation to GEA or LA because of the putative added value of these two products. Their low maximum achievable yields begged the question whether other products of GEOR should be pursued. Specifically, different mechanistic pathways, upon further oxidation of intermediate C_3 and C_2 products, lead to the common C_1 product of formate (FA; Fig. S1). Hence, we applied the RSM approach to conceptually explore possible outcomes of simultaneous maximization of current density and Faradaic efficiency to formate (FA).

The RSM model obtained for simultaneous optimization of CD and FE to FA predicted a maximum CD of 177 mA cm^{-2} and maximum FE to FA of 50% at factor settings of $[\text{GLY}] = 1.82 \text{ M}$, $[\text{NaOH}] = 3.22 \text{ M}$, $\text{CL} = 0.72 \text{ mg cm}^{-2}$, and $\text{EFR} = 1.71 \text{ ml min}^{-1}$ (Table S12). As expected, these responses are much higher than the optimized CDs and FEs for C_3 products (increases of over 60 and 145 mA cm^{-2} in CD and of 27% and 20% in FE compared with GEA and LA, respectively). RSCs for simultaneous optimization of CD and FE to FA indicate that all four factors meaningfully influenced the responses (Fig. S2), and as such we plot the simulated responses (CD and FE to FA) against each other to quantitatively interpret the multi-objective optimization (Fig. 9a). The ranges of

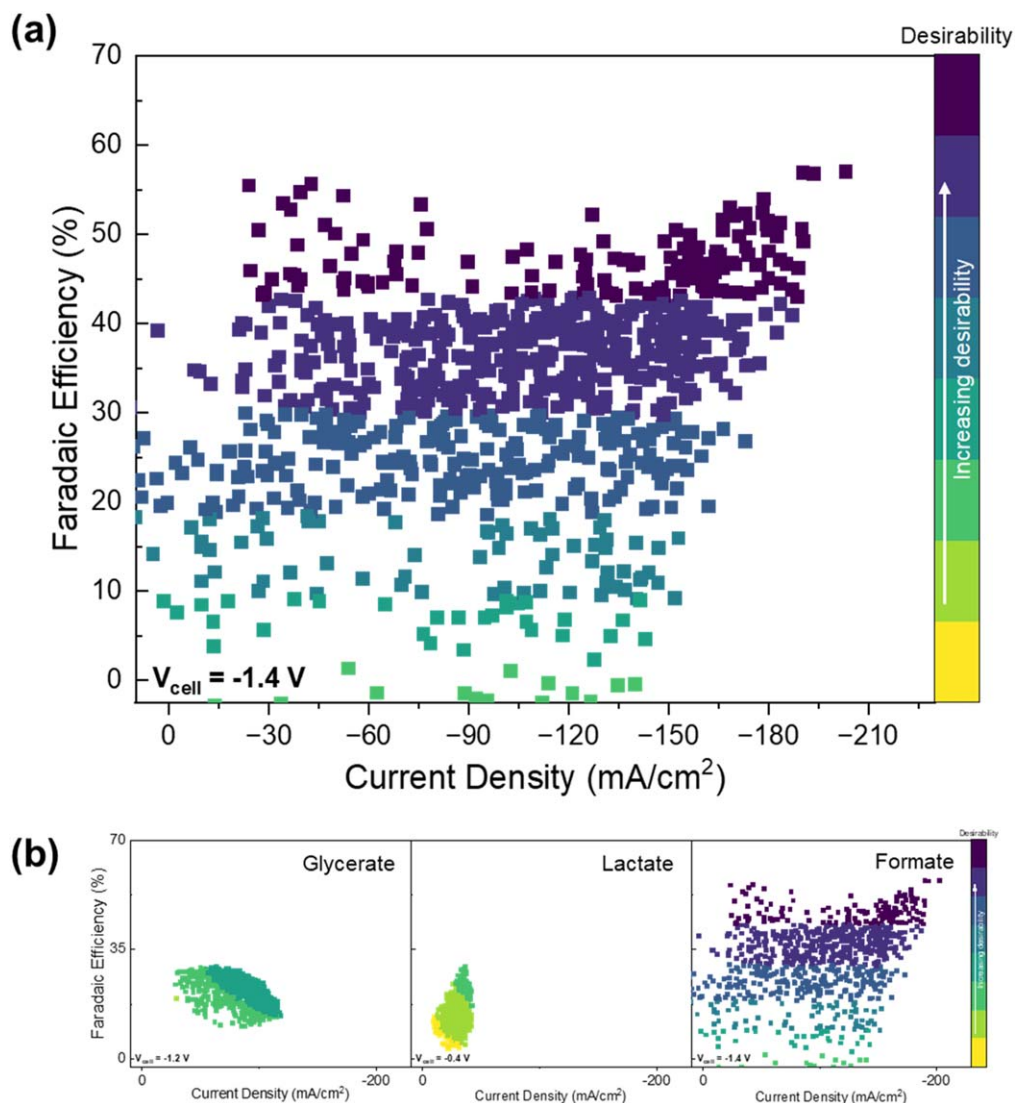


Figure 9. (a) Pareto front for simultaneous optimization of current density and Faradaic efficiency to formate. This figure is colored differently than Fig. 8 to underscore the vastly different scales; a direct comparison can be seen in Fig. S3. While formate is a less-valuable product than glycerate or lactate, the reaction is not limited by [NaOH] or chemical decomposition and can reach over 200 mA cm^{-2} current density and over 50% Faradaic efficiency. These responses well exceed that which can be achieved by optimizing for C_3 products. (b) Comparison of optimizations for Faradaic efficiencies to glycerate, lactate, and formate on the same scales. Formate has the widest range of current density and Faradaic efficiency, as well as the highest desirabilities.

CD, FE to FA, *and* desirability are double those of GEA. Because the scales are vastly different, we have colored them differently than the data shown in Fig. 8. Figure 9b highlights the vastly different ranges of accessible combinations of CD and FE to X for GEA, LA, and FA: the very different achievable maximum values for each, and the broad range of accessible combinations for FA. Clearly, simultaneously maximizing CD and FE to FA is more straightforward, and results in more industrially relevant CD and FE than optimizing for production of a C_3 product like GEA and LA. Formate and its corollary products (C_2 compounds oxalate, glycolate, and acetate) may provide a pathway for optimization that produces a binary, easily-separable mixture with high selectivity *and* high activity simultaneously.

Conclusions

In sum, this work utilized the framework of a Response Surface Methodology design of experiments to efficiently evaluate the influence of [NaOH], [glycerol], catalyst loading, and electrolyte flow rate on current density (activity) and Faradaic efficiency (selectivity) of the glycerol electrooxidation reaction. Applying this framework

to the predetermined factor ranges ([NaOH] = [GLY] = [0.01, 4 M]; CL = [0.1–1.0 mg cm^{-2}]; EFR = [0.5–2.0 ml min^{-1}]) yielded a set of 30 distinct conditions, which were then experimentally evaluated at 7 cell potentials. The experimental data was then fed back to the software to produce a training set, which generated models for optimizing current density alone, optimizing Faradaic efficiency to a particular product only, or optimizing current density and Faradaic efficiency simultaneously. The model was then used to generate response coefficients, simulated runs (here 1000), and optimal operating conditions. Model outcomes were validated using confirmation experiments for all three optimization goals. The combined graphical representations of these model outcomes and experimental data were then evaluated and interpreted in the context of GEOR, which revealed insights beyond those that could have been obtained using a traditional p-value approach alone. Specifically:

- [NaOH] and [GLY] are the two most important factors in optimizing overall *current density* but are relevant in different ways. Maximizing current density occurred at [NaOH] > 2.5 M and $1 \text{ M} \leq [\text{GLY}] \leq 3 \text{ M}$.

- Product speciation pathways for the C_3 products *lactate* and *glycerate* are controlled primarily by [NaOH], with some influence of EFR, in line with prior mechanistic understanding. Specifically, increasing [NaOH] and decreasing EFR increases the prevalence of the E-C (E-E) pathway to lactate (and vice versa for glycerate). Maximizing Faradic efficiency to lactate: [NaOH] > 3.5 M, 1 M ≤ [GLY] ≤ 3 M, and EFR ≤ 1.25 ml min⁻¹. Maximizing Faradic efficiency to glycerate: [NaOH] < 0.5 M, 1 M ≤ [GLY] ≤ 3 M, EFR > 1.25 ml min⁻¹; both at -0.4 V cell potential.

- Higher current densities can be achieved when optimizing current density and Faradic efficiency to glycerate vs current density and Faradic efficiency to lactate. On first sight, this was surprising, as maximizing current density and maximizing Faradic efficiency to glycerate have opposite [NaOH] requirements (high for current density, low for Faradic efficiency to glycerate). However, reasonable (>20%) Faradic efficiencies to glycerate can be achieved at higher cell potentials, whereas reasonable Faradic efficiencies to lactate can only occur at lower cell potentials that suppress further reaction and side product formation. Optimization for a product that can be synthesized at higher cell potentials, such as glycerate, is more desirable for overall cell performance because higher cell potentials most typically increase current density.

- Investigation of the simultaneous optimization of current density and Faradic efficiency to *formate* revealed achievable current densities above 200 mA cm⁻² and Faradaic efficiencies above 50% (performance more appropriate for scaling) despite formate being a less-valuable product with a smaller market than either glycerate or lactate.

Notably, the above insights obtained using RSCs, simulated runs, etc. could not be derived using a p-value analysis alone, because the latter arbitrarily assigns “significance” to factors but provides no further insight on the responses’ sensitivity to those factors (RSCs) or on the overall appearance of the parameter space (simulated runs). For example, p-value analysis would have discarded the model of Faradic efficiency to lactate entirely, such that no meaningful speciation evaluation could be performed. Models of complex systems need to be evaluated thoughtfully and holistically in the context of the reactions and processes they represent.

To truly assess the potential of GEOR as an economically feasible process to synthesize different or specific products, more considerations of greater breadth must be made. For instance, the cost of product separation must be factored in. Processes needed to separate many of these mixtures of low molecular weight acids have not been developed, and/or have not been evaluated in terms of economic feasibility (including energy consumption) at scale. Based on the outcomes of the work here, one would expect that separating a binary mixture of predominantly formate and a corollary C_2 product to be less costly than separating a mixture of multiple similar products (and unreacted glycerol) produced under the conditions of optimizing Faradic efficiency for either glycerate or for lactate.

This study only considered GEOR on Au. Other catalysts can be evaluated in a similar manner. Both non-noble catalysts and homogenous (solution-phase) redox mediators hold promise for GEOR, as they cannot be over-oxidized and thus deactivated; however, the mechanisms of GEOR on these catalysts are different from the GEOR mechanism of noble catalysts such as Au. Applying RSM to GEOR using catalysts such as Ni and redox mediators such as TEMPO may enable synthesis of higher-value products under high current density regimes.

This work employed a microfluidic liquid electrolyte flow reactor. Scaling GEOR beyond the benchtop may require moving to membrane electrode assembly (MEA)-type electrolysis cell configurations that may affect the experimental outcomes (achievable current densities, Faradic efficiencies). Further research can elucidate such differences resulting from electrolysis cell configuration and operational regimes.

Most importantly, assessment of opportunities for scaling GEOR to a sustainable, electrified manufacturing method for certain value-

added products will require a critical evaluation of the feedstock. In this work, 99.9% pure glycerol was used, whereas in envisioned application of GEOR at scale, the feedstock would be an industrial waste stream frequently referred to as “crude glycerol.” The glycerol content in “crude” rarely passes 80% purity, with the remainder of the solution usually comprising methanol, NaOH, and water. A detailed assessment of how this purity affects GEOR performance in the three key dimensions of activity, selectivity, and stability is crucial to establish the scope of GEOR for electrified chemical manufacturing. Future investigations of GEOR should consider the various aforementioned factors to optimize activity, product selectivity, stability, and cost.

In sum, this work reported an accessible and interpretable framework for integrating experimental electroanalysis and statistical modeling insights of complex electrochemical systems. While this study focused on the glycerol electrooxidation reaction, the methodology should be broadly applicable to other systems to efficiently investigate their multidimensional parameter spaces.

Experimental

Preparation of electrolytes and solvents.—All electrolyte solutions of varying compositions and concentrations were prepared by dissolving the appropriate amounts of NaOH (Ward’s Science, reagent grade) and/or glycerol (Fisher Chemical, certified ACS) into deionized water. 0.5 M and 5 mM H₂SO₄ (Sigma Aldrich, ACS reagent, 95.0%-98.0%) for HPLC analysis were prepared in the same manner.

Preparation and imaging of electrodes.—The anode (cathode) electrocatalysts are comprised of Au (Pt) deposited using a sputter system with DC argon plasma (Orion 3, AJA) on gas diffusion electrodes (GDEs; Freudenberg H23C6, Fuel Cell Store). Actual catalyst loading was determined by weighing the GDEs before and after deposition. All cathode (Pt) loadings were 1.0 ± 0.1 mg cm⁻². The targeted anode (Au) loading varied with the experimental conditions generated by the analysis software; targeted loadings and actual loadings can be found in Tables I and S1. All Au loadings were within 10% of the targeted loading. SEM/EDX (Axia ChemiSEM, Thermo Fisher Scientific) was performed to characterize the electrodes (Table S5, Figs. S4–5). Prior to imaging, catalysts were rinsed thoroughly with deionized water and dried under nitrogen, as described previously.⁶⁴ Images were taken at 5,000x or 10,000x magnification and a working distance of approximately 16 mm. Acceleration voltage of 20.00 kV was used at a pressure of 0.005 Pa. Image resolution was set to 768 × 512 and each image was acquired for 30 s. All images are presented without color-correction and without aspect-ratio alteration; however, images have been cropped for ease of viewing. All information cropped from the images is reported above.

Electrochemical flow reactor operation.—We utilize a liquid electrolyte flow cell with single-pass flow, similar to previous work.^{65,66} This electrolyzer is of the same dimensions as described previously, and includes two PEEK liquid electrolyte flow channels separated by an anion exchange membrane (Fumasep Fumion FAA-PK-75, Fuel Cell Store). Both the anode and cathode gas compartments are closed to the atmosphere, such that the gas generated must flow out of the cell in the same manner as the liquid electrolyte and products. The cell is operated at ambient temperature and pressure. Reference electrodes (RE-5B, Ag/AgCl, BASi) were placed upstream of the flow cell and connected individually to measure half-cell potentials. The potentials in this study are reported without any IR correction.

We collected experimental data for 7 sets of 30 experiments. Current density data were obtained using a potentiostat (Reference 600, Gamry) by allowing the system to equilibrate for one minute, then averaging over the last three minutes of each experiment and dividing by exposed geometric area of electrode (1 cm²). For the last

two minutes of each experiment, anolyte effluent was collected in a vial (with total volume collected dependent on the flow rate tested). 0.5 ml of the collected effluent was immediately acidified with 0.5 ml of 0.5 M H₂SO₄ to limit further base-catalyzed chemical reactions. Total experiment time at each set of experimental conditions thus took four minutes.

Product analysis.—Prior to experimentation, 0.5 ml of unused anolyte was collected and acidified to determine the solution baseline composition for HPLC analysis, as glycerol in alkaline media will react slowly to some of the products also formed during electrooxidation.⁵⁹ All liquid products were analyzed using high-performance liquid chromatography using an ion exclusion column with diluted H₂SO₄ mobile phase flowed at 0.6 ml min⁻¹ (Shimadzu Nexera; Bio-Rad Aminex HPX 87H; 5 mM H₂SO₄). Column temperature was maintained at 60 °C and separated products were detected with a UV–vis detector. Faradaic efficiencies were obtained from the raw HPLC data using a MATLAB script for maximum consistency and accuracy of spectral integration, with mathematics following prior work.⁶⁷ The MATLAB script was derived from resources developed by O’Haver,⁶⁸ and is available upon request.

Factor and factor range determination.—Most sources of industrial waste glycerol streams contain a significant fraction of NaOH.⁶⁹ Thus, we elected to use NaOH as the electrolyte salt required for conductivity, reactivity, and alkalinity. A 2 M NaOH solution was used as the catholyte. Control experiments flowing 4 M NaOH in the catholyte (anolyte) and 0.01 M NaOH in the anolyte (catholyte) at 0.5 ml min⁻¹ for 10 min, under an applied potential of -1.6 V, showed negligible changes in solution conductivity. Because these tests were run at conditions more extreme than any of the experimental conditions used in this study, we concluded that electrolyte crossover between the anolyte and catholyte does not occur to a significant degree, and thus any difference in ionic strength between anolyte and catholyte does not affect the experimental outcomes.

To determine the operating ranges of our cell, a series of cell failure tests was conducted (Fig. S3). Cell failure in the context of this study equals so-called “flooding,” where electrolyte solution permeates the hydrophobic microporous layer and carbon-fiber substrate of the gas diffusion electrode and seeps out into the gas chambers on either side of the electrolysis cell. This phenomenon has been described in prior work.^{70,71} For the study reported here, we identified the range of operational conditions over which flooding can be avoided or minimized. Key factors included electrolyte viscosity, flow rate, and composition. Viscosity was measured on solutions of anolyte (NaOH, glycerol, and DI water) ranging from [NaOH] = [GLY] = 0.01 M to [NaOH] = [GLY] = 7 M, and those solutions were then evaluated in the liquid electrolyte flow cell at electrolyte flow rates (EFRs) from 0.5–2.0 ml min⁻¹. At EFR = 2.0 ml min⁻¹, the cell failed with any solution viscosity beyond 5 cP (corresponding to [NaOH] = [GLY] ≈ 4 M). Beyond this limit of 10 cP ml min⁻¹, the liquid electrolyte flow cell flooded. Because of this limit, increasing EFR beyond 2.0 ml min⁻¹ was impractical, as it severely curtailed the operational range of [NaOH] and [GLY]. For practical reasons, the lower limit of EFR was set at 0.5 ml min⁻¹, so sufficient electrolyte (1 mL) could be collected in the 2 min effluent collection time during each experiment. Thus, we set the EFR range to [0.5 ml min⁻¹, 2.0 ml min⁻¹] and NaOH] = [GLY] = [0.01 M, 4.0 M] to encompass the widest possible range of operating conditions that avoid flooding-related problems. A catalyst loading (CL) range of [0.1 mg cm⁻²–1.0 mg⁻¹ cm⁻²] was used, with the upper limit set by the sputter system used. A loading of 1 mg cm⁻² roughly corresponds to 590 nm of Au deposited on our electrodes, within the 600 nm system limit.

RSM model setup.—To create the experimental training set described in this study, we used JMP Pro 17 software and its inbuilt

Response Surface Design DOE script. Inputting our factor ranges and desired responses (*vide supra*) into the script generated the experimental training set. After inputting experimental results into the script, the model is generated by performing polynomial linear regression (PLR). PLR uses a line of best fit to evaluate the experimental data and generates the rest of the information used to evaluate the model, such as response surface coefficients (RSCs) and optimum points. The complete set of results for each optimization (CD; FE to GEA or to LA; and both) can be found in the Supplementary Information (Tables S5–S10).

RSM model evaluation.—In accordance with statistical best practices,^{61,72–74} all models were evaluated for their statistical robustness prior to analysis in the Results & Discussion. To identify models suitable for analysis, lack-of-fit p-values were evaluated *in the context of the optimization*. Significant lack-of-fit p-values (<0.05) indicate models where additional factors are needed to explain model behavior. In our optimization for current density alone, all sub-models showed a significant lack-of-fit. This is to be expected, as we did not include any factors related to current density from the cathodic hydrogen evolution reaction. However, we held our cathodic factors constant (apart from EFR, which was varied in tandem to maintain consistent electrode wetting). EFR was not the most influential contributor in any sub-model. Furthermore, ionic strength did not influence results (*vide supra*). Thus, in accordance with the guidance of the American Statistical Association (*vide supra*), these lack-of-fit p-values can be reasonably ignored. For Faradaic efficiency to glycerate, however, lack-of-fit p-values were identified for only *some* of the sub-models: -0.2 V, -0.8 V, and -1.4 V. For -0.2 V, the prevalence of chemical reactions during the electrolysis process likely overshadow the electrolytic reaction; similarly, for -1.4 V, contributions from the onset of the oxygen evolution reaction are likely influences on product speciation variation. In contrast, the origin of the lack of fit at -0.8 V in the model is less clear. It is possible that HPLC chromatogram deconvolution is more complex at this intermediate potential, where the extent of the reaction is less well-controlled. To ensure that the data was interpreted solely on the basis of electrochemical reactions and was not influenced by inconsistencies in data analysis or other concurrent reactions, *all three of these potentials were excluded* from the analysis of Faradaic efficiencies and the analysis of the multi-objective (current density and Faradaic efficiency simultaneously) optimizations.

To ensure the model gave sensible predictions, leverage-based extrapolation control was used. In essence, utilizing leverage-based extrapolation control limits our predictions to areas where our *predicted* responses do not deviate from the mean more than *actual* responses deviate from the mean seen in the data set. Leverage is defined as the quantification of the influence of the observed response on its predicted value and is a measure of the distance between a particular data point’s response and the average of the responses for all data points. As an example, in our data set, the *leverage* for experiment X’s current density equals (experiment X’s current density) minus (the average of current densities for all experiments). For leverage-based extrapolation control, the maximum extrapolation threshold is set as the maximum leverage. Thus, we cannot extrapolate any value beyond the maximum value of leverage.

The models were also evaluated on their balance (lack or presence of skew), using maximum correlation of estimates (COE) and the variance inflation factor (VIF), which are typically interpreted together. Both VIF and COE indicate whether collinearity is present. Collinearity is defined as correlation between two factors (x-variables), such that they cannot independently predict the value of the response (y-variable). If two factors are collinear, they each explain some of the variation in *each other*, instead of in the response. Both are directly related to the imprecision in generating “real-world” factors; for example, both COE and VIF are increased

when using a solution of concentration 1.05 M instead of the model-generated 1.047786 M. Interpreting both factors together provides insight into the overall skew present in the model.

COE calculates the theoretical correlation of each regression coefficient and depends on the predictor values and the intercept term generated in the model. Generally, COEs less than 0.3 indicate little to no imbalance; between 0.3 and 0.5 indicate some, but an acceptable amount of imbalance; and values from 0.5 to 1 show a high amount of imbalance that requires further inspection. All models generated show a COE of 0.5712 (Tables S5–S7). To ascertain whether our models were able to provide reliable predictions, we evaluated VIFs. VIFs quantify how much the variance of a regression coefficient is increased due to its factor's correlation to other variables; the square root of a VIF describes the increase in standard error of a factor's coefficients from interactions with other factors relative to the standard error of the factor's coefficients if they had no correlation to other factors. For example, a VIF of 4 indicates that the standard error of the response surface coefficient is twice as large as the coefficient that does not interact with other factors. Generally, VIFs less than 5 are considered to show low model imbalance, while VIFs greater than 5 show high model imbalance. All models generated in this study had VIFs less than 1.5, indicating low model imbalance (Tables S5–S7). The low VIFs combined with the high COEs indicate that, indeed, the RSM models for CD, FE, and CD & FE simultaneously, are imperfect, but acceptable for analysis. Likely, the high COEs stem primarily from the variance in HPLC data discussed throughout the text (*vide supra*); the low VIFs indicate that the variance in “real-world” factor values from those generated by the models (i.e., using 1.5, rather than 1.48729) do not add much imbalance. This highlights the importance of binary or easily separable mixtures, as quantification of large numbers of products can introduce problems in modeling a system.

Acknowledgments

The authors acknowledge funding from the National Science Foundation through the EFRI-DChEM program, grant #2029326 (Renewable-Energy Driven Electrocatalytic Co-Conversion of CO₂ and Regional Feedstocks to Chemicals and Fuels) and a TechnipFMC fellowship to RNG. We also acknowledge the use of facilities and instrumentation supported by NSF through the University of Illinois Materials Research Science and Engineering Center DMR-2309037. The basis code for the MATLAB scripts used for HPLC chromatogram analysis were generously provided by Tom O'Haver, University of Maryland-College Park. We also appreciate helpful feedback and many fruitful conversations with Raghuram Gaddam, Adam Sibal, Joaquín Rodríguez-López, and Ashlynn Stillwell.

ORCID

Rachel N. Gaines <https://orcid.org/0000-0003-1953-0194>
 Beth A. Kleimenhagen <https://orcid.org/0009-0006-1249-103X>
 James J. Griebler <https://orcid.org/0000-0002-1056-4593>
 Andrew A. Gewirth <https://orcid.org/0000-0003-4400-9907>
 Simon A. Rogers <https://orcid.org/0000-0002-3432-5044>
 Paul J. A. Kenis <https://orcid.org/0000-0001-7348-0381>

References

1. F. W.-S. Lucas, R. G. Grim, S. A. Tacey, C. A. Downes, J. Hasse, A. M. Roman, C. A. Farberow, J. A. Schaidle, and A. Holewinski, “Electrochemical routes for the valorization of biomass-derived feedstocks: from chemistry to application.” *ACS Energy Lett.*, **6**, 1205 (2021).
2. E. J. Biddinger and P. J.-A. Kenis, “Current and emerging electrochemical approaches for chemical manufacturing.” *Electrochem. Soc. Interface*, **32**, 41 (2023).
3. M. R. Anuar and A. Z. Abdullah, “Challenges in biodiesel industry with regards to feedstock, environmental, social and sustainability issues: a critical review.” *Renew. Sustain. Energy Rev.*, **58**, 208 (2016).
4. S. Verma, S. Lu, and P. J.-A. Kenis, “Co-electrolysis of CO₂ and glycerol as a pathway to carbon chemicals with improved technoeconomics due to low electricity consumption.” *Nat. Energy*, **4**, 466 (2019).
5. A. Badreldin, E. Youssef, A. Djire, A. Abdala, and A. Abdel-Wahab, “A critical look at alternative oxidation reactions for hydrogen production from water electrolysis.” *Cell Reports Physical Science*, **4**, 101427 (2023).
6. Y. Li, X. Wei, L. Chen, and J. Shi, “Electrocatalytic hydrogen production trilogy.” *Angew. Chem. Int. Ed.*, **60**, 19550 (2021).
7. C. Coutanceau, S. Baranton, and R. S.-B. Kouamé, “Selective electrooxidation of glycerol into value-added chemicals: a short overview.” *Front. Chem.*, **7**, 1 100 (2019).
8. M. Simões, S. Baranton, and C. Coutanceau, “Electrochemical valorisation of glycerol.” *ChemSusChem*, **5**, 2106 (2012).
9. A. C. Brix et al., “Electrocatalytic oxidation of glycerol using solid-state synthesised nickel boride: impact of key electrolysis parameters on product selectivity.” *Chem. Electro. Chem.*, **8**, 2336 (2021).
10. S. Chornaja, S. Zhizhukun, K. Dubencovs, O. Stepanova, E. Spröge, V. Kampars, L. Kulikova, V. Serga, A. Cvetkovs, and E. Palcevskis, “New methods of glyceric and lactic acid production by catalytic oxidation of glycerol. new method of synthesis of a catalyst with enhanced activity and selectivity.” *Chemija*, **26**, 113–119 (2015), <https://ortus.rtu.lv/science/en/publications/21257>.
11. C. Dai, L. Sun, H. Liao, B. Khezri, R. D. Webster, A. C. Fisher, and Z. J. Xu, “Electrochemical production of lactic acid from glycerol oxidation catalyzed by AuPt nanoparticles.” *J. Catal.*, **356**, 14 (2017).
12. C. S. Lee, M. K. Aroua, W. A. Wan Daud, P. Cognet, Y. Pérès, and M. A. Ajeel, “Selective electrochemical conversion of glycerol to glycolic acid and lactic acid on a mixed carbon-black activated carbon electrode in a single compartment electrochemical cell.” *Front. Chem.*, **7**, 1 110 (2019).
13. Y. Li, S. Chen, J. Xu, H. Zhang, Y. Zhao, Y. Wang, and Z. Liu, “Ni promoted Pt and Pd catalysts for glycerol oxidation to lactic acid.” *CLEAN—Soil, Air, Water*, **42**, 1140 (2014).
14. S. Lux, P. Stehring, and M. Siebenhofer, “Lactic acid production as a new approach for exploitation of glycerol.” *Sep. Sci. Technol.*, **45**, 1921 (2010).
15. G. Melle, M. B.-C. de Souza, P. V.-B. Santiago, P. G. Corradini, L. H. Mascaro, P. S. Fernández, and E. Sitta, “Glycerol electro-oxidation at pt in alkaline media: influence of mass transport and cations.” *Electrochim. Acta*, **398**, 139318 (2021).
16. N. Y. Suzuki, P. V.-B. Santiago, T. S. Galhardo, W. A. Carvalho, J. Souza-Garcia, and C. A. Angelucci, “Insights of glycerol electrooxidation on polycrystalline silver electrode.” *J. Electroanal. Chem.*, **780**, 391 (2016).
17. R. Boukili, N. Tuleushova, D. Cot, B. Rebiere, V. Bonniol, J. Cambedouzou, S. Tingry, D. Cornu, and Y. Holade, “Enhanced electrocatalytic activity and selectivity of glycerol oxidation triggered by nanoalloyed silver–gold nanocages directly grown on gas diffusion electrodes.” *J. Mater. Chem. A*, **8**, 8848 (2020).
18. Z. Zhang, L. Xin, J. Qi, Z. Wang, and W. Li, “Selective electro-conversion of glycerol to glycolate on carbon nanotube supported gold catalyst.” *Green Chem.*, **14**, 2150 (2012).
19. M. S.-E. Houache, E. Cossar, S. Ntais, and E. A. Baranova, “Electrochemical modification of nickel surfaces for efficient glycerol electrooxidation.” *J. Power Sources*, **375**, 310 (2018).
20. Y. Kwon, K. J.-P. Schouten, and M. T.-M. Koper, “Mechanism of the catalytic oxidation of glycerol on polycrystalline gold and platinum electrodes.” *Chem. Cat. Chem.*, **3**, 1176 (2011).
21. J. Zhang and Y. Shen, “Electro-oxidation of glycerol into formic acid by nickel-copper electrocatalysts.” *J. Electrochem. Soc.*, **168**, 084510 (2021).
22. J. L. Bott-Neto, T. S. Martins, S. A.-S. Machado, and E. A. Ticianelli, “Electrocatalytic oxidation of methanol, ethanol, and glycerol on Ni(OH)₂ nanoparticles encapsulated with Poly[Ni(Salen)] film.” *ACS Appl. Mater. Interfaces*, **11**, 30810 (2019).
23. J. B. Costa Santos, C. Vieira, R. Crisafulli, and J. J. Linares, “Promotional effect of auxiliary metals Bi on Pt, Pd, and Ag on Au, for glycerol electrolysis.” *Int. J. Hydrogen Energy*, **45**, 25658 (2020).
24. M. S.-E. Houache, K. Hughes, R. Safari, G. A. Botton, and E. A. Baranova, “Modification of nickel surfaces by bismuth: effect on electrochemical activity and selectivity toward glycerol.” *ACS Appl. Mater. Interfaces*, **12**, 15095 (2020).
25. G. Wang et al., “Cost-effective and durable electrocatalysts for Co-electrolysis of CO₂ conversion and glycerol upgrading.” *Nano Energy*, **92**, 106751 (2022).
26. M. S. Ahmad, C. K. Cheng, R. Kumar, S. Singh, K. A. Saeed, H. R. Ong, H. Abdullah, and M. R. Khan, “Pd/CNT catalysts for glycerol electro-oxidation: effect of Pd loading on production of valuable chemical products.” *Electroanalysis*, **32**, 1139 (2020).
27. V. Del Colle, L. M.-S. Nunes, C. A. Angelucci, J. M. Feliu, and G. Tremiliosi-Filho, “The influence of stepped Pt(111)×(110) electrodes towards glycerol electrooxidation: electrochemical and FTIR studies.” *Electrochim. Acta*, **346**, 136187 (2020).
28. A. C. Garcia, M. J. Kolb, C. van Nierop y Sanchez, J. Vos, Y. Y. Birdja, Y. Kwon, G. Tremiliosi-Filho, and M. T.-M. Koper, “Strong impact of platinum surface structure on primary and secondary alcohol oxidation during electro-oxidation of glycerol.” *ACS Catal.*, **6**, 4491 (2016).
29. H. J. Kim et al., “Coproducing value-added chemicals and hydrogen with electrocatalytic glycerol oxidation technology: experimental and techno-economic investigations.” *ACS Sustainable Chem. Eng.*, **5**, 6626 (2017).
30. J. Schnaidt, M. Heinen, D. Denot, Z. Jusys, and R. Jürgen Behm, “Electrooxidation of glycerol studied by combined in situ IR spectroscopy and online mass spectrometry under continuous flow conditions.” *J. Electroanal. Chem.*, **661**, 250 (2011).
31. Y. Zhou, Y. Shen, and X. Luo, “Optimizing the activity and selectivity of glycerol oxidation over core-shell electrocatalysts.” *J. Catal.*, **381**, 130 (2020).

32. X. Jin, M. Zhao, C. Zeng, W. Yan, Z. Song, P. S. Thapa, B. Subramaniam, and R. V. Chaudhari, "Oxidation of glycerol to dicarboxylic acids using cobalt catalysts." *ACS Catal.*, **6**, 4576 (2016).
33. S. Schünemann, F. Schüth, and H. Tüysüz, "Selective glycerol oxidation over ordered mesoporous copper aluminum oxide catalysts." *Catal. Sci. Technol.*, **7**, 5614 (2017).
34. J. Wu, X. Liu, Y. Hao, S. Wang, R. Wang, W. Du, S. Cha, X.-Y. Ma, X. Yang, and M. Gong, "Ligand hybridization for electro-reforming waste glycerol into isolable oxalate and hydrogen." *Angew. Chem. Int. Ed.*, **62**, e202216083 (2023).
35. J. F. Gomes and G. Tremiliosi-Filho, "Spectroscopic studies of the glycerol electro-oxidation on polycrystalline Au and Pt surfaces in acidic and alkaline media." *Electrocatal.*, **2**, 96 (2011).
36. Y. Holade, C. Morais, K. Servat, T. W. Napporn, and K. B. Kokoh, "Toward the electrochemical valorization of glycerol: Fourier transform infrared spectroscopic and chromatographic studies." *ACS Catal.*, **3**, 2403 (2013).
37. C. A. Ottoni, S. G. da Silva, R. F.-B. De Souza, and A. O. Neto, "PtAu electrocatalyst for glycerol oxidation reaction using a ATR-FTIR/single direct alkaline glycerol/air cell in situ study." *Electrocatalysis*, **7**, 22 (2016).
38. Z. Zhang, L. Xin, J. Qi, D. J. Chadderton, K. Sun, K. M. Warsko, and W. Li, "Selective electro-oxidation of glycerol to tartronate or mesoxalate on a nanoparticle catalyst via electrode potential tuning in anion-exchange membrane electro-catalytic flow reactor." *Appl. Catalysis B*, **147**, 871 (2014).
39. M. S.-E. Houache, K. Hughes, A. Ahmed, R. Safari, H. Liu, G. A. Botton, and E. A. Baranova, "Electrochemical valorization of glycerol on Ni-rich bimetallic NiPd nanoparticles: insight into product selectivity using in situ polarization modulation infrared-reflection absorption spectroscopy." *ACS Sustainable Chem. Eng.*, **7**, 14425 (2019).
40. R. G. Da Silva, S. Aquino Neto, K. B. Kokoh, and A. R. De Andrade, "Electroconversion of glycerol in alkaline medium: from generation of energy to formation of value-added products." *J. Power Sources*, **351**, 174 (2017).
41. T. Noël, Y. Cao, and G. Laudadio, "The fundamentals behind the use of flow reactors in electrochemistry." *Acc. Chem. Res.*, **52**, 2858 (2019).
42. J. White, L. Peters, D. Martín-Yerga, I. Terekhina, A. Anil, H. Lundberg, M. Johansson, G. Salazar-Alvarez, G. Henriksson, and A. Cornell, "Glycerol electrooxidation at industrially relevant current densities using electrodeposited PdNi/nifoam catalysts in aerated alkaline media." *J. Electrochem. Soc.*, **170**, 086504 (2023).
43. B. Endrődi, G. Bencsik, F. Darvas, R. Jones, K. Rajeshwar, and C. Janáky, "Continuous-flow electroreduction of carbon dioxide." *Prog. Energy Combust. Sci.*, **62**, 133 (2017).
44. M. Jouny, W. Luc, and F. Jiao, "General techno-economic analysis of CO₂ electrolysis systems." *Ind. Eng. Chem. Res.*, **57**, 2165 (2018).
45. S. Verma, B. Kim, H.-R.-M. Jhong, S. Ma, and P. J.-A. Kenis, "A gross-margin model for defining techno-economic benchmarks in the electroreduction of CO₂." *ChemSusChem*, **9**, 1972 (2016).
46. A. J. Martín, G. O. Larrazábal, and J. Pérez-Ramírez, "Towards sustainable fuels and chemicals through the electrochemical reduction of CO₂: lessons from water electrolysis." *Green Chem.*, **17**, 5114 (2015).
47. C. A. Angelucci, H. Varela, G. Tremiliosi-Filho, and J. F. Gomes, "The significance of non-covalent interactions on the electro-oxidation of alcohols on Pt and Au in alkaline media." *Electrochem. Commun.*, **33**, 10 (2013).
48. M. Etesami and N. Mohamed, "Catalytic application of gold nanoparticles electrodeposited by fast scan cyclic voltammetry to glycerol electrooxidation in alkaline electrolyte." *Int. J. Electrochem. Sci.*, **6**, 4676 (2011).
49. D. M. Morales, D. Jambrec, M. A. Kazakova, M. Braun, N. Sikdar, A. Koul, A. C. Brix, S. Seisel, C. Andronescu, and W. Schuhmann, "Electrocatalytic conversion of glycerol to oxalate on Ni oxide nanoparticles-modified oxidized multiwalled carbon nanotubes." *ACS Catal.*, **12**, 982 (2022).
50. A. Yuksel, H. Koga, M. Sasaki, and M. Goto, "Hydrothermal electrolysis of glycerol using a continuous flow reactor." *Ind. Eng. Chem. Res.*, **49**, 1520 (2010).
51. J. F. Gomes, C. A. Martins, M. J. Giz, G. Tremiliosi-Filho, and G. A. Camara, "Insights into the adsorption and electro-oxidation of glycerol: self-inhibition and concentration effects." *J. Catal.*, **301**, 154 (2013).
52. N. Yahya, S. K. Kamarudin, N. A. Karim, M. S. Masdar, and K. S. Loh, "Enhanced performance of a novel anodic PdAu/VGCNF catalyst for electro-oxidation in a glycerol fuel cell." *Nanoscale Res. Lett.*, **12**, 605 (2017).
53. D. Panjiara and H. Pramanik, "Optimization of process parameters using response surface methodology (RSM) for power generation via electrooxidation of glycerol in T-shaped air breathing microfluidic fuel cell (MFC)." *Int. J. Hydrogen Energy*, **45**, 33968 (2020).
54. A. Khosravanipour Mostafazadeh, M. S. De La Torre, Y. Padilla, P. Drogui, S. K. Brar, R. D. Tyagi, Y. Le Bihan, G. Buelna, and P. G. Moroyoqui, "An insight into an electro-catalytic reactor concept for high value-added production from crude glycerol: optimization, electrode passivation, product distribution, and reaction pathway identification." *Renewable Energy*, **172**, 130 (2021).
55. E. Peralta-Reyes, D. Vizcarreta-Vásquez, R. Natividad, A. Aizpuru, E. Robles-Gómez, C. Alanis, and A. Regalado-Méndez, "Electrochemical reforming of glycerol into hydrogen in a batch-stirred electrochemical tank reactor equipped with stainless steel electrodes: parametric optimization, total operating cost, and life cycle assessment." *J. Environ. Chem. Eng.*, **10**, 108108 (2022).
56. *NIST/SEMATECH e-Handbook of Statistical Methods*, **5.3.3.6**, Response surface designs (accessed 2023-10-27).
57. S. S. Bhargava, F. Proietto, D. Azmoodeh, E. R. Cofell, D. A. Henckel, S. Verma, C. J. Brooks, A. A. Gewirth, and P. J.-A. Kenis, "System design rules for the electrochemical reduction of CO₂ to CO on Ag nanoparticles." *Chem. Electro. Chem.*, **7**, 2001 (2020).
58. R. Green, R. Brown, and D. Pletcher, "Understanding the performance of a microfluidic electrolysis cell for routine organic electrosynthesis." *Journal of Flow Chemistry*, **5**, 31 (2014).
59. Y. Kwon, S. C.-S. Lai, P. Rodriguez, and M. T.-M. Koper, "Electrocatalytic oxidation of alcohols on gold in alkaline media: base or gold catalysis?" *J. Am. Chem. Soc.*, **133**, 6914 (2011).
60. G. Qin, X. Wang, X. Wan, D. Chen, and B. Qiu, "Nanotubes TiO₂ supported Pt catalyst for selective electrocatalytic oxidation of glycerol to glyceric acid." *Energy Sources Part A*, **42**, 2120 (2020).
61. R. L. Wasserstein and N. A. Lazar, "The ASA statement on P-values: context, process, and purpose." *The American Statistician*, **70**, 129 (2016).
62. L. Pérez-Martínez, L. Balke, and A. Cuesta, "Reactive and inhibiting species in the electrocatalytic oxidation of glycerol on gold: a study combining in-situ visible reflectance and ATR-SEIRAS." *J. Catal.*, **394**, 1 (2021).
63. A. M. Verma, L. Laverdure, M. M. Melander, and K. Honkala, "Mechanistic origins of the pH Dependency in Au-catalyzed glycerol electro-oxidation: insight from first-principles calculations." *ACS Catal.*, **12**, 662 (2022).
64. E. R. Cofell, Z. Park, U. O. Nwabara, L. C. Harris, S. S. Bhargava, A. A. Gewirth, and P. J.-A. Kenis, "Potential cycling of silver cathodes in an alkaline CO₂ flow electrolyzer for accelerated stress testing and carbonate inhibition." *ACS Appl. Energy Mater.*, **5**, 12013 (2022).
65. M. S. Naughton, A. A. Moradia, and P. J.-A. Kenis, "Quantitative analysis of single-electrode plots to understand in-situ behavior of individual electrodes." *J. Electrochem. Soc.*, **159**, B761 (2012).
66. S. Verma, X. Lu, S. Ma, R. I. Masel, and P. J.-A. Kenis, "The effect of electrolyte composition on the electroreduction of CO₂ to CO on Ag based gas diffusion electrodes." *Phys. Chem. Chem. Phys.*, **18**, 7075 (2016).
67. M. K. Goetz, M. T. Bender, and K.-S. Choi, "Predictive control of selective secondary alcohol oxidation of glycerol on NiOOH." *Nat. Commun.*, **13**, 5848 (2022).
68. T. O'Haver, *A Pragmatic Introduction to Signal Processing* (2023), <https://terpconnect.umd.edu/~toh/spectrum/IntroToSignalProcessing.pdf> (accessed 2023-12-13).
69. F. Yang, M. A. Hanna, and R. Sun, "Value-added uses for crude glycerol—a byproduct of biodiesel production." *Biotechnol. Biofuels*, **5**, 1 (2012).
70. U. O. Nwabara, E. R. Cofell, S. Verma, E. Negro, and P. J.-A. Kenis, "Durable cathodes and electrolyzers for the efficient aqueous electrochemical reduction of CO₂." *Chem. Sus. Chem.*, **13**, 855 (2020).
71. U. O. Nwabara, M. P. De Heer, E. R. Cofell, S. Verma, E. Negro, and P. J.-A. Kenis, "Towards accelerated durability testing protocols for CO₂ electrolysis." *J. Mater. Chem. A*, **8**, 22557 (2020).
72. J. Sall, A. Lehman, M. Stephens, and S. Loring, *JMP® Start Statistics: A Guide to Statistics and Data Analysis Using JMP®* (SAS Institute Inc., Cary, NC) Sixth ed. (2017).
73. B. Govaerts, B. Franq, R. Marion, M. Martin, and M. Thiel, "1.16 - The essentials on linear regression, ANOVA, general linear and linear mixed models for the chemist." In *Comprehensive Chemometrics*, ed. S. Brown et al. (Elsevier: Oxford) (Second Edition) ed. 431 (2020).
74. R. H. Myers, D. C. Montgomery, and C. M. Anderson-Cook, *Response Surface Methodology: Process and Product Optimization Using Designed Experiments* (Wiley) (2016).